



PERGAMON

Journal of the Mechanics and Physics of Solids
50 (2002) 1051–1077

JOURNAL OF THE
MECHANICS AND
PHYSICS OF SOLIDS

www.elsevier.com/locate/jmps

Three-dimensional constitutive model for shape memory alloys based on microplane model

M. Brocca, L.C. Brinson*, Z.P. Bažant

Departments of Civil and Mechanical Engineering, Northwestern University, Evanston, IL 60208-3111, USA

Received 27 September 2000; accepted 18 August 2001

Abstract

A new model for the behavior of polycrystalline shape memory alloys (SMA), based on a statically constrained microplane theory, is proposed. The new model can predict three-dimensional response by superposing the effects of inelastic deformations computed on several planes of different orientation, thus reproducing closely the actual physical behavior of the material. Due to the structure of the microplane algorithm, only a one-dimensional constitutive law is necessary on each plane. In this paper, a simple constitutive law and a robust kinetic expression are used as the local constitutive law on the microplane level. The results for SMA response on the macroscale are promising: simple one-dimensional response is easily reproduced, as are more complex features such as stress–strain subloops and tension–compression asymmetry. A key feature of the new model is its ability to accurately represent the deviation from normality exhibited by SMAs under nonproportional loading paths. © 2002 Elsevier Science Ltd. All rights reserved.

Keywords: Shape memory alloys; Constitutive relations; Plasticity; Microplane model

1. Introduction and background

Shape memory alloys (SMA) are materials capable of very large recoverable inelastic strain (of the order of 10%). For this property they have been extensively investigated over the past three decades as potential control materials. The source of the distinctive mechanical behavior of these materials is a crystalline phase transformation between a high symmetry, highly ordered parent phase (*austenite*), and a low symmetry, less ordered product phase (*martensite*).

* Corresponding author. Fax: +1-847-463-0540.

E-mail address: cbrinson@northwestern.edu (L.C. Brinson).

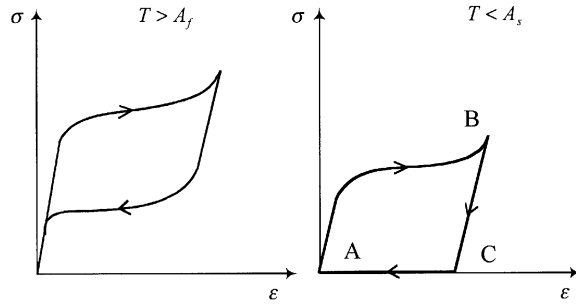


Fig. 1. Pseudoelasticity (a) and shape memory effect (b) for a SMA material.

Martensitic structure is obtained from austenite with application of mechanical load or decrease in temperature. Upon heating or reduction of stress, the austenitic structure is recovered. This is the cause of the two most significant phenomena that characterize the mechanical behavior of SMAs: the pseudoelastic response and the shape memory effect (SME). To illustrate the macroscale manifestation of these phenomena, typical uniaxial stress–strain diagrams for a polycrystalline SMA material are shown in Fig. 1.

In absence of stress, the start and finish transformation temperatures are typically denoted as M_s , M_f , A_s , A_f . For many materials, $M_f < M_s < A_s < A_f$. At a temperature $T > A_f$, a SMA material behaves pseudoelastically (Fig. 1(a)). Applying stress induces transformation of austenite into martensite, resulting in inelastic transformation strain. As the stress is reduced, after an initial elastic response the martensite formed during the loading process transforms back to austenite, the inelastic strain is therefore recovered, and the stress–strain diagram exhibits the characteristic hysteretic loop shown in Fig. 1(a).

Fig. 1(b) illustrates the shape memory effect for material starting as austenite at a temperature $T < A_s$. During the loading process (A \rightarrow B), the applied stress induces formation of martensite and inelastic strain. Upon unloading from B to C, the newly formed martensite remains stable, as does the transformation strain. Upon heating the material to temperatures above A_f , the material becomes again completely austenitic and the inelastic strain is fully recovered (C \rightarrow A).

To determine what crystallographic state is stable at a given combination of applied uniaxial stress and temperature, a phase diagram depicting the critical stress for the phase transformation as a function of temperature can be used. A simplified typical phase diagram is shown in Fig. 2 (the phase diagram and transformation kinetics will be revisited in more detail in Section 4). Transformation from austenite to martensite can take place in the [M] strip between the two lines with slope C_M , passing through M_f and M_s . Transformation from martensite to austenite can take place in the [A] strip between the two lines with slope C_A , passing through A_s and A_f . A phase diagram for a particular alloy is derived experimentally by performing several uniaxial tests at different temperatures.

Even for uniaxial loading, other complicated combinations of pseudoelasticity and SME are often the subject of in-depth study. Experimental results for one-dimensional

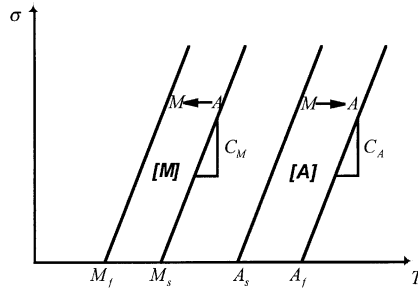


Fig. 2. Simplified schematic for inelastic domains of $A \rightarrow M$ and $M \rightarrow A$ transformations. Distinction between detwinned (stress-induced) and twinned (temperature-induced) martensite not represented here (see later Fig. 6).

thermomechanical loading histories are discussed in numerous papers on SMA materials published in the last three decades. Issues such as transformation return points, partial transformations and hysteresis subloop formation have been considered (Ivshin and Pence, 1994a,b; Lu et al., 1990; Tanaka et al., 1995a,b, 1996).

Pseudoelasticity and the shape memory effect make SMAs very appealing as potential materials for various engineering applications. It is advantageous that the transformation temperatures can be controlled by the alloying elements that constitute the material. This allows the designer to exploit the properties of SMAs over a wide range of temperatures. Among several other applications, SMAs are used to produce shrink fit rings (Borden, 1996), actuators (in the form of torque bars or wires, Otsuka and Wayman, 1998), orthodontic wires and other medical devices (Auricchio, 1995; Otsuka and Wayman, 1998). SMAs are also useful as dampers, thanks to the energy dissipated in the pseudoelastic hysteresis (Graesser and Cozzarelli, 1991; Oberaigner et al., 1996; Lagoudas et al., 1994; Boyd and Lagoudas, 1996a,b). In practical applications, SMAs are often used in the form of wires. This caused the attention of experimental researchers to be mostly focused on one-dimensional behavior, and several constitutive models capable of satisfactorily reproducing one-dimensional response of SMA have been developed (see references in Section 2). However, finite element analysis in design of advanced applications of SMAs requires the knowledge of fully three-dimensional constitutive laws. SMAs are often subjected to triaxial stress states, for instance, when embedded in other materials to enhance the damping properties of composite structures.

To fully understand shape memory response, one must move from the purely macroscopic description given above to a more detailed microscale viewpoint. Fig. 3 (after Otsuka and Wayman, 1998) illustrates schematically how the transformation strain can be produced and then recovered crystallographically. Fig. 3(a) shows a simplified austenitic single crystal. Upon cooling at zero stress, martensite plates nucleate and grow inside the austenite until, at $T < M_f$, the material is completely martensitic. Martensite formed in such a manner assumes a self-accommodated structure in which the combination of variants does not produce a macroscopic observable strain (Fig. 3(b)). The stress applied to a self-accommodated martensitic structure, however,

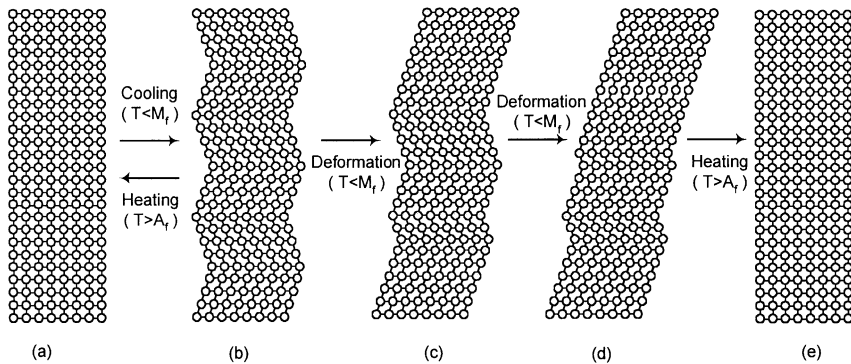


Fig. 3. Mechanism of shape memory effect (after Otsuka and Wayman, 1998).

induces a large, macroscopic deformation due to reorientation of martensite variants (*detwinning*) (Fig. 3(c) and (d)).

When the temperature is increased again above A_f , the martensite gradually transforms back to austenite with the original crystallographic orientation, thus allowing for a full recovery of the detwinning strain (Fig. 3(e)). Polycrystalline response is similar with each individual grain in the polycrystal responding to its local stress and temperature state, as described above. The overall polycrystal response is an averaged response over all the differently oriented single crystal grains.

Following this simple introduction to the mechanical behavior of SMA materials, Section 2 will briefly review the existing one-dimensional (1-D) and three-dimensional (3-D) SMA models and motivate the development of the proposed microplane model. It will be shown that the statically constrained microplane model is a very efficient numerical framework for the development of a macroscale three-dimensional SMA model and offers exciting potential for further development of SMA models at the micro and meso scales. Section 3 will review microplane model approach, while Section 4 will present the formulation for macroscale prediction of polycrystalline SMA response. Section 5 will give numerical predictions with the usual 1-D response replication, plus more complicated subloop phenomena, as well as illustrate the capability of the model to capture SMA response under nonproportional loading.

2. Review of existing 1- and 3-D SMA models

The macroscopic mechanical behavior of shape memory alloys is usually modeled following either a phenomenological or a micromechanical approach.

2.1. Macroscopic phenomenological models

One-dimensional phenomenological models are suitable for engineering practice, because they make use of measurable quantities as parameters and are often relatively simple. These models are often ad hoc descriptions aimed at fitting experimental data and are usually quite accurate in predicting the uniaxial response of SMAs.

Uniaxial phenomenological models have been proposed by many researchers, among them Tanaka and Nagaki (1982), Liang and Rogers (1990), Ivshin and Pence (1994a, b) and Brinson (1993).

These models usually consist of a mechanical law, governing the stress–strain behavior, and a kinetic law, governing the crystallographic transformation. The kinetic laws employed in these models describe the evolution of the phase fraction as a function of stress and temperature and often make use of a phase diagram such as that shown in Fig. 3.

As discussed by Brinson and Huang (1996), the main factor distinguishing these one-dimensional models is the particular kinetic law. This is due to the fact that the transformation strain is very large compared to the elastic strain, and therefore the mechanical part of the model plays a less significant role. Brinson and Huang showed that several different models yield very similar results when the same kinetic law is used.

Several attempts are being made to extend these models to three dimensions. 3-D phenomenological models appear to be capable of capturing the typical features of SMAs, but it is difficult to evaluate the performance of 3-D phenomenological models due to the lack of experimental data for multiaxial response. The existing 3-D models are developed in the form of plasticity models with an internal variable such as the *phase fraction* ξ (Boyd and Lagoudas, 1994; Lubliner and Auricchio, 1996; Liang and Rogers, 1992; Lagoudas et al., 1996; Birman, 1997) and most have been compared directly only to uniaxial experimental data.

2.2. Micromechanics based macroscopic models

The researchers following a micromechanics approach (Sun and Hwang, 1993; Paatoor et al., 1988, 1993, 1994; Goo and Lexcellent, 1997; Huang and Brinson, 1998; Gao et al., 2000; Vivet and Lexcellent, 1998; Lu and Weng, 1997) try in various ways to follow very closely the crystallographic phenomena within the material, using thermodynamics laws to describe the transformation. These models often consider the martensitic variants as transforming inclusions and use micromechanics to calculate the interaction energy due to the phase transformation in the material. Stresses and strains are obtained as volume averages calculated over a volume in which many inclusions are considered, representing the possible variants.

The models conceived following this approach are obviously much more complicated than phenomenological models and usually are computationally demanding. On the other hand, being based on an accurate investigation of the physics of the material, these models seem to offer the most rational way to derive a highly accurate three-dimensional constitutive law.

2.3. A microplane model for SMA

A *microplane model* for SMA, proposed in this paper, falls in between the two approaches just mentioned. As will be described in the following section, the microplane model is in essence a phenomenological model, which aims at reproducing the

macroscopic mechanical behavior of materials. But while in the usual phenomenological models the constitutive laws are expressed directly in terms of stress and strain tensors and their invariants, in a microplane model the macroscopic material behavior is obtained by describing the material response along several planes of different orientations, called the microplanes. While not directly modeling material microstructure, use of multiple microplanes is considered to be generally representative of microstructural response, thereby allowing a more direct and intuitive description of phenomena occurring at the microscale level. The stress and strain quantities on the microplanes have an immediate physical meaning such as shear strain, normal pressure on the plane or shear stress along the plane, and thus these quantities can be used to describe phenomena such as crystallographic slip, shear bands, crack opening, friction, etc.

The phenomena occurring at the microplane level contribute jointly to the overall macroscopic response of the material. When the material response can be approximated as isotropic, the constitutive laws for the microplane response can be assumed to be the same on all the microplanes. This reduces the task of developing a three-dimensional constitutive law to the much simpler task of identifying relationships to describe the material response on a plane. In some cases (as for the SMA model proposed in this paper), a simple one-dimensional constitutive law at the microplane level is sufficient to generate a consistent three-dimensional model.

We stress, however, that the number and orientations of the microplanes are dictated by numerical considerations, as will be seen in the next section, and thus the microplanes are not intended to give an accurate microscopic and crystallographic description of the material microstructure (as some of the strict micromechanics SMA models do). In fact, the constitutive laws at the microplane level must be phenomenological laws, to compensate for the possible discrepancy between the microplane structure and the material microstructure. Although there is potential to apply the microplane model more directly at the microscale level by choosing the microplanes based on known habit plane orientations for a given SMA, such an approach is left for future work. In this paper, the microplane model approach will be used to develop a constitutive model for polycrystalline SMA materials based on macroscale phenomenological constitutive laws for the microplanes.

The main advantages in the proposed approach arise from the fact that by allowing the material laws to be prescribed independently on several planes, the model is quite versatile and capable of reproducing phenomena difficult to capture with the traditional models expressed in terms of stress and strain tensors and their invariants. For example, recently Lim and McDowell (1999) have shown experimentally that a constitutive law based on a J_2 -type transformation rule (such as that used for von Mises or Drucker Prager yield surfaces) is not accurate in the case of nonproportional multiaxial loading of an SMA. By performing experiments on SMAs under axial torsional nonproportional loading, Lim and McDowell showed that the direction of transformation strain is not colinear with the deviatoric stress (as it would be in a J_2 -type formulation). This finding increases the interest in the microplane model, which naturally exhibits deviation from normality; indeed, independent contributions from numerous planes produce a multi-surface plasticity type of response in the material, with vertex effect (see Brocca and Bažant, 2000). In addition to this, the microplane model is rather intuitive and

therefore it is relatively easy to modify and tune to given data simply by changing the constitutive laws at the microplane level. It will be shown that important SMA characteristics such as pressure sensitivity and tension–compression asymmetry can be easily introduced in the model.

3. The microplane model approach

3.1. History of microplane model

The history of the microplane modeling approach can be traced back to a pioneering idea of Taylor (1938), who proposed characterizing the constitutive behavior of polycrystalline metals by relations between the stress and strain vectors acting on planes of all possible orientations within the material and determining the macroscopic strain and stress tensors as a summation of all these vectors under the assumption of a static or kinematic constraint. Batdorf and Budiansky (1949) were the first to extend Taylor's idea and develop a realistic model for plasticity of polycrystalline metals, still considered among the best. Many other researchers subsequently refined or modified this approach to metals (Kröner, 1961; Budiansky and Wu, 1962; Lin and Ito, 1965, 1966; Hill, 1965, 1966; Rice, 1971). Extensions for the hardening inelastic response of soils and rocks were also made (Zienkiewicz and Pande, 1977; Pande and Sharma, 1983; Pande and Xiong, 1982).

All the aforementioned models used the so-called “static constraint”—the assumption that the stress vector acting on a given plane in the material, called the microplane, is the projection of the macroscopic stress tensor. Later, Bažant (1984), and Bažant and Oh (1985) showed that a static constraint prevents the model from being generalized for postpeak behavior or damage of quasi-brittle materials. The extension to softening damage requires replacing the static constraint by a kinematic constraint, in which the strain vector or any inclined plane in the material is the projection of the macroscopic strain tensor.

In all applications to metals, the formulations emanating from Taylor's and Batdorf and Budiansky's work were called the “slip theory of plasticity”. However, this expression is unsuitable for general material models (Bažant and Prat, 1988a,b), for example models of the damage in quasi-brittle materials, where the inelastic behavior on the microscale does not physically represent slip. For this reason, the neutral term “microplane model” was coined, applicable to any type of inelastic behavior (Bažant, 1984). Microplane is the name given to a plane of any orientation in the material, used to approximately characterize the behavior in the microstructure of the material.

After generalizing the microplane model for both tensile and compressive damage (Bažant and Prat, 1988a,b), the microplane model and the corresponding numerical algorithm reached its present, very effective formulation for concrete in Bažant et al. (2000). Microplane formulations have also been developed for anisotropic clays (Bažant and Prat, 1987) and for soils (Prat and Bažant, 1989, 1991a,b). A detailed review of the microplane model formulation with kinematic or static constraint can be found in Carol and Bažant (1997). For both the formulation with kinematic constraint and the

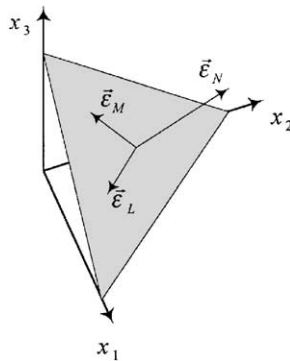


Fig. 4. Strain components on a microplane.

formulation with static constraint, the material properties are characterized by relations between the stress and strain components on the microplanes. The tensorial invariance restrictions need not be directly enforced in the constitutive relations, which is a simplifying feature of the microplane formulation. They are automatically satisfied by superimposing in a suitable manner the responses from the microplanes of all orientations. This is done by means of a variational principle (principle of virtual work) (Bažant, 1984).

3.2. Formulation with kinematic constraint

The orientation of a microplane is characterized by the unit normal \mathbf{n} of components n_i (indices i and j refer to the components in Cartesian coordinates x_i). In the formulation with a kinematic constraint, which makes it possible to describe softening in a stable manner, the strain vector $\vec{\varepsilon}_N$ on the microplane (Fig. 4) is the projection of the macroscopic strain tensor ε_{ij} . So the components of this vector are $\varepsilon_{Ni} = \varepsilon_{ij}n_j$. The normal strain on the microplane is $\varepsilon_N = n_i\varepsilon_{Ni}$, that is

$$\varepsilon_N = N_{ij}\varepsilon_{ij}, \quad N_{ij} = n_in_j, \quad (3.1)$$

where repeated indices imply summation over $i = 1, 2, 3$. The mean normal strain, called the volumetric strain ε_V , and the deviatoric strain ε_D on the microplane can also be introduced, defined as follows:

$$\varepsilon_V = \varepsilon_{kk}/3, \quad \varepsilon_D = \varepsilon_N - \varepsilon_V. \quad (3.2)$$

This separation of ε_V and ε_D is useful when the effect of the hydrostatic components of stress and strain needs to be controlled directly, or when the volumetric–deviatoric interaction observed for a number of cohesive frictional materials, such as concrete, needs to be captured. We will not need to use ε_V and ε_D for the model presented in Section 4: the effect of hydrostatic pressure will be taken into account indirectly as will be explained later.

To characterize the shear strains on the microplane (Fig. 4), we need to define two coordinate directions M and L , given by two orthogonal unit coordinate vectors \mathbf{m} and \mathbf{l} of components m_i and l_i lying on the microplane. To minimize directional bias of \mathbf{m} and \mathbf{l} among microplanes, we alternate among choosing vectors \mathbf{m} to be normal to axis x_1 , x_2 and x_3 .

The magnitudes of the shear strain components on the microplane in the directions of \mathbf{m} and \mathbf{l} are $\varepsilon_M = m_i(\varepsilon_{ij}n_j)$ and $\varepsilon_L = l_i(\varepsilon_{ij}n_j)$. Because of the symmetry of tensor ε_{ij} , the shear strain components may be written as follows (e.g. Bažant et al., 1996, 1999):

$$\varepsilon_M = M_{ij}\varepsilon_{ij}, \quad \varepsilon_L = L_{ij}\varepsilon_{ij}, \quad (3.3)$$

in which the following symmetric tensors were introduced:

$$M_{ij} = (m_in_j + m_jn_i)/2, \quad L_{ij} = (l_in_j + l_jn_i)/2. \quad (3.4)$$

Once the strain components on each microplane are obtained, the stress components are updated through microplane constitutive laws, which can be expressed in algebraic or differential forms. In this paper, these microplane constitutive laws are taken to be an appropriate version of an existing 1-D SMA constitutive model as described in Section 4.

If the kinematic constraint is imposed, the stress components on the microplanes are equal to the projections of the macroscopic stress tensor σ_{ij} only in some particular cases, when the microplane constitutive laws are specifically prescribed in a manner such that this condition be satisfied. This happens for example in the case of elastic laws at the microplane level, defined with elastic constants chosen so that the overall macroscopic behavior be the usual elastic behavior (see Carol and Bažant, 1997). In general, the stress components determined independently on the various microplanes will not be related to one another in such a manner that they can be considered as projections of a macroscopic stress tensor. Thus, the static equivalence or equilibrium between the microlevel stress components and macrolevel stress tensor must be enforced by other means. This can be accomplished (as proposed in Bažant, 1984) by application of the principle of virtual work, yielding

$$\sigma_{ij} = \frac{3}{2\pi} \int_{\Omega} \sigma_N n_i n_j \, d\Omega + \frac{3}{2\pi} \int_{\Omega} \frac{\sigma_{Tr}}{2} (n_i \delta_{rj} + n_j \delta_{ri}) \, d\Omega, \quad (3.5)$$

where Ω is the surface of a unit hemisphere. Eq. (3.5) is based on the equality of the virtual work inside a unit sphere and on its surface, rigorously justified by Bažant et al. (1996).

The integration in Eq. (3.5), is performed numerically by Gaussian integration using a finite number of integration points on the surface of the hemisphere. Such an integration technique corresponds to considering a finite number of microplanes, one for each integration point. A formula consisting of 28 integration points is given by Stroud (1971). Bažant and Oh (1986) developed a more efficient and nearly equally accurate formula with 21 integration points, and studied the accuracy of various formulas in different situations.

3.3. Formulation with static constraint

A formulation with static constraint equates the stress components on each microplane to the projections of the macroscopic stress tensor σ_{ij} . Once the strain components on each microplane are updated by use of the microplane constitutive laws, the macroscopic strain tensor is obtained again by applying the principle of virtual work.

The microplane components of stress are defined as follows:

$$\sigma_N = N_{ij}\sigma_{ij}, \quad N_{ij} = n_i n_j, \quad (3.6)$$

$$\sigma_M = M_{ij}\sigma_{ij}, \quad \sigma_L = L_{ij}\sigma_{ij}. \quad (3.7)$$

The complementary work equation, dual to Eq. (3.5), can be written as

$$\varepsilon_{ij} = \frac{3}{2\pi} \int_{\Omega} \varepsilon_N n_i n_j \, d\Omega + \frac{3}{2\pi} \int_{\Omega} \frac{\varepsilon_{Tr}}{2} (n_i \delta_{rj} + n_j \delta_{ri}) \, d\Omega. \quad (3.8)$$

Again, volumetric and deviatoric quantities could be introduced:

$$\sigma_V = \sigma_{kk}/3, \quad \sigma_D = \sigma_N - \sigma_V. \quad (3.9)$$

Although they will not be needed in the model presented in the next section, σ_V and σ_D are useful when the effect of hydrostatic pressure and volumetric–deviatoric interaction must be accounted for explicitly.

3.4. Formulation with double constraint

It is possible and advantageous to formulate the microplane model with particular material laws such that a kinematic constraint for the strains coexists with a static constraint for the true stresses in the sense of damage mechanics (but of course not with the actual stresses). When this happens the model is said to have a *double constraint* and it satisfies simultaneously integral equations (3.5) for strains and Eq. (3.8) for true stresses. Such a double constraint is useful in microplane damage formulations (Carol and Bažant, 1997; Bažant et al., 1996, 2000).

3.5. Overall application

Fig. 5 shows schematically the pattern followed in order to update the stress or strain in the microplane model approach. As seen, the microplane model takes a one-dimensional constitutive law on each microplane and transforms this into a consistent three-dimensional model. In this work, the static constraint is used. Thus, the macroscale stress tensor is projected onto the 28 microplanes using Eqs. (3.6) and (3.7). A 1-D constitutive law and kinetic law for SMAs (described in the next section) is applied on each microplane along with a combined constraint on total martensite fraction, producing the strains on each of the 28 microplanes. The macroscopic strain is then determined numerically via integration of Eq. (3.8). The numerical procedure is incremental and small increments in stress are taken at each step.

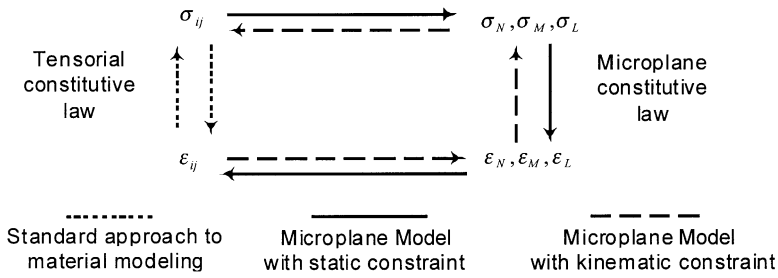


Fig. 5. Patterns for stress or strain update in the microplane model with static or kinematic constraint.

4. Microplane constitutive model for SMA

The main objective of this paper is to formulate a microplane model for SMA constitutive behavior. Several simplifications will be introduced, and refinements of the model as well as alternate approaches are left to future studies. In the present model, no rate effect due to latent heat is considered, thermal expansion is neglected, and the elastic modulus of the material is considered to be independent of the martensite fraction. Furthermore, the volumetric response is taken as elastic and the effect of the hydrostatic pressure on the martensitic transformation is not directly addressed. However, the model will be able to take into account the effect of hydrostatic pressure indirectly, achieved through a dependence of the microplane kinetic law on the normal component of stress on each plane (see Section 4.4).

To implement the microplane model, one needs to prescribe on each plane only a one-dimensional constitutive law, to describe the shear response in each of two chosen reference directions normal to each other, namely those characterized by vectors \mathbf{m} and \mathbf{l} . Note that the same constitutive law is used for both directions. Admittedly, this approach introduces a certain directional bias within each microplane and invariance with respect to rotation of vectors \mathbf{m} and \mathbf{l} does not hold. This difficulty could be avoided by considering a 2-D yield surface for the resulting shear vector on each microplane (which has been tried for concrete). However, by choosing vectors \mathbf{m} and \mathbf{l} randomly on each microplane (and also at each integration point of the finite element model), the biases effectively cancel out and the model is almost invariant in the overall sense. This approach makes the model computationally simpler without any significant loss of accuracy.

The transformation of an SMA single crystal can be represented by a shear strain induced by shear stress such that at the microstructural level only the shear transformation strain contributes significantly to the overall inelastic strain. The overall response of a polycrystalline material, however, is a superposition of the shear contributions in the many differently oriented single crystal grains. Given this picture of material response, one can see two scales at which a microplane model for SMA constitutive behavior could be applied: (1) at the microscale (single crystal) level, with each microplane representing a habit plane of martensite; in this case, the microplane orientations would

necessarily be dictated by the known crystallographic transformation planes, the microplane constitutive laws would be dictated by the known transformation strains for each variant, and the overall model would simulate response of a SMA single crystal. (2) At the macroscale (polycrystal) level, with the microplane model being used as a consistent and efficient approach to transition from a one-dimensional constitutive model for shear of a polycrystal to a three-dimensional model for general loading; in this case, the microplane orientations can be chosen for numerical efficiency. This paper pursues this latter approach and the overall model simulates the response of an SMA polycrystal.

Since the SMA transformation is fundamentally in shear at the microscale level, it is appropriate for our macroscale model to utilize an SMA constitutive model valid for shear deformation as the local constitutive law at the microplane level. When the only source of inelastic deformation is the shear strain on the microplanes, as it is in this case, the kinematic constraint poses some limitations to the material compliance (Brocca and Bažant, 2000). We therefore use a statically constrained microplane model, which calculates the stress components on each microplane from the stress tensor and the local SMA constitutive law then provides the shear strain on each microplane. The constitutive law used here is analogous to those that followed the initial proposal by Tanaka in the 1980s outside the microplane context. In particular, the present model will be adapted to the form of the constitutive law proposed by Brinson (1993), with some simplifications.

4.1. SMA constitutive law

On each microplane, the shear deformation can be assumed to be governed in general by the following 1-D law:

$$\sigma - \sigma_0 = E(\varepsilon - \varepsilon_0) + \Omega(\xi - \xi_0) + \Theta(T - T_0), \quad (4.1)$$

where σ is the shear stress and ε is the shear strain in either of the directions \mathbf{m} and \mathbf{l} ; ξ is the martensite fraction, E is the elastic modulus, Ω is usually called the “transformation tensor” (although a scalar quantity in 1-D), and Θ is related to the thermal coefficient of expansion for the material; $(\sigma_0, \varepsilon_0, \xi_0, T_0)$ represent the initial state of the material.

It has been shown (Brinson and Huang, 1996) that constitutive law (4.1) can be more simply expressed as

$$\sigma = E(\varepsilon - \varepsilon_L \xi) + \Theta \Delta T, \quad (4.2)$$

where ε_L is the maximum transformation strain. In the application here, we will neglect the thermal expansion term, simplifying the expression further to

$$\sigma = E(\varepsilon - \varepsilon_L \xi). \quad (4.3)$$

Note that here ξ represents the *stress-induced* martensitic fraction: the fraction of the material that has been transformed by stress into a single martensitic variant and is therefore associated directly with a transformation strain, not the overall percentage of the material transformed to martensite. A distinction between *temperature-induced*

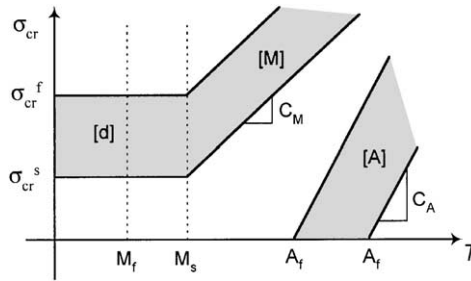


Fig. 6. Critical stresses for transformation or martensite twin conversion as functions of temperature (from Brinson). We are careful here to represent regions of transformation to stress-induced martensite (associated with transformation strain) which cause the difference from the schematic in Fig. 2.

martensite, with multiple variants, and *stress-induced* martensite has been introduced by Brinson (1993) and subsequently adopted by other researchers (e.g., Auricchio and Sacco, 1999; Govindjee and Hall, 2000; Wu and Pence, 1998). This distinction is necessary to have a constitutive equation that is valid for temperatures below M_s as well as above.

4.2. SMA kinetic law

The constitutive equation (4.3) must be combined with a kinetic law, which governs the evolution of ξ as a function of the thermomechanical loading history.

To describe the algorithm used to enforce the kinetic law, we will refer to the phase diagram shown in Fig. 6, which gives the variation with temperature of the stresses for transformation to detwinned (stress-induced) martensite or to austenite. The critical values of stress for conversion of martensite variants below M_s are assumed to be constant. In the following, we will explicitly consider only the $[M]$ region of the forward martensitic transformation strip, but as noted in Bekker and Brinson (1998) $[d]$ can be treated in exactly the same fashion and simply accommodated. In the present study, we need only the evolution equations for the calculation of the stress-induced martensite fraction. The stress σ in the phase diagram of Fig. 6 is either σ_L or σ_M in our model and the critical stresses represented on the diagram are the shear stresses required for stress-induced martensitic transformation on a microplane. Fig. 6 shows only the part of the phase diagram for positive values of σ . The complete diagram (shown in Fig. 9) is symmetric with respect to the temperature axis, to reflect the fact that there is no preferential direction for the transformation strain on a given microplane.

Whenever a point representative of the thermomechanical state on a microplane enters the shaded area on the diagram of Fig. 6, ξ must be updated. An efficient and reliable algorithm is needed to ensure that ξ is always continuous and bounded within the interval $[0, 1]$. The thermomechanical path can be complex, as in the example shown in Fig. 7, or it can consist of cycles. The algorithm employed to update ξ must be able to consistently reproduce the path dependence of martensitic transformation. The model proposed in the present study will adopt an algorithm analogous to that

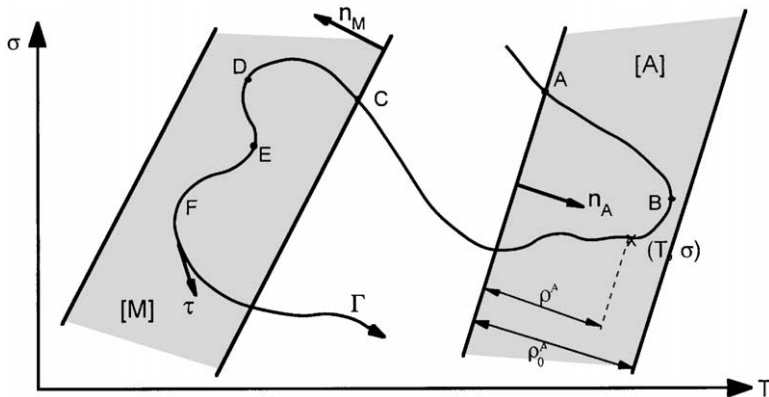


Fig. 7. A loading path Γ with several switching points indicated by solid circles. Current stress state used to define distances ρ_0^i and ρ^i in the $[A]$ strip indicated by x .

proposed by Bekker and Brinson (1998), who introduced a procedure based on the geometry of the loading path on the stress–temperature phase diagram. For a rigorous formulation of the kinetic law, see the original paper by Bekker and Brinson. Here we will give only a brief presentation of the concepts on which the algorithm is based.

Fig. 7 shows a loading path Γ and a portion of the phase diagram. The normal vectors \vec{n}_A and \vec{n}_M represent the directions of transformation change in the $[A]$ and $[M]$ strips, respectively. At any point on the path, $\vec{\tau}$ is the vector tangent to Γ . A transformation occurs whenever one of the following conditions is satisfied:

$$\begin{aligned}
 & \text{(a) } \vec{\tau} \cdot \vec{n}_A > 0 \quad \text{in } [A], \\
 & \text{(b) } \vec{\tau} \cdot \vec{n}_M > 0 \quad \text{in } [M].
 \end{aligned}
 \tag{4.4}$$

A given loading path Γ can be subdivided into several segments ($\Gamma_n, n = 1, 2, \dots$) by introducing the *switching points*, defined as the points where the direction or sense of the transformation changes. The switching points can be points where Γ enters or leaves the transformation strip in the direction of transformation (points A and C in Fig. 7), or points inside the strip where the dot product between $\vec{\tau}$ and \vec{n}_A or \vec{n}_M changes sign (points B, D, E, F in Fig. 7). Along the portions of Γ between two switching points, ξ is monotonically either increasing or decreasing (when moving in a transformation direction, e.g. between C and D) or constant (when moving opposite to the transformation direction, e.g. between D and E).

A global kinetic law for the whole path can be given as a sequence of local kinetic laws for the portions Γ_n . Bekker and Brinson present three ways to formulate the local kinetic law, one of which is utilized here. We first define $Y^i = Y^i(T, \sigma), (i = A, M)$ as the normalized distance between a given point on Γ inside a transformation strip and the start boundary. Y^i is given by the following expression:

$$Y^i = \frac{\rho^i}{\rho_0^i},
 \tag{4.5}$$

where ρ^i is the distance of point (T, σ) from the start boundary, and ρ_0^i is the width of the strip. Fig. 7 illustrates these quantities for the case of the $[M]$ strip.

On a given portion Γ_n between two switching points, ξ can then be updated using the appropriate one of the following expressions:

$$\xi = \xi_j f^A(Y^A - Y_j^A) \quad (4.6)$$

when the point is inside the $[A]$ strip, and

$$\xi = \xi_j + (1 - \xi_j) f^M(Y^M - Y_j^M) \quad (4.7)$$

when the point is inside the $[M]$ strip.

In the forgoing expressions, quantities marked with subscript j are the values of the martensite fraction and the normalized distance at the previous switching point relevant to the current transformation, ξ is the stress-induced martensite fraction and f^j are interpolation functions. Here cosine interpolation functions are used, equivalent to those originally developed by Liang and Rogers (1990):

$$f^A(Y^A - Y_j^A) = 1 - \frac{1}{2} \{1 - \cos[\pi(Y^A - Y_j^A)]\}, \quad (4.8)$$

$$f^M(Y^M - Y_j^M) = \frac{1}{2} \{1 - \cos[\pi(Y^M - Y_j^M)]\}. \quad (4.9)$$

Note that Eqs. (4.6)–(4.9) are derived empirically and might need to be adapted when used for different SMA materials. The microplane model developed here is not dependent on this particular form of the kinetic expressions and could easily accommodate alternate kinetic laws.

4.3. Microplane implementation

The SMA microplane model is implemented using the statically constrained microplane formulation to project the macroscopic stress state onto each microplane (Eqs. (3.6) and (3.7)). The SMA constitutive and kinetic laws (Eqs. (4.3), (4.6)–(4.9)) are used as the local constitutive law for shear on each microplane. Then the overall shear strain is obtained using Eq. (3.8). The calculation is performed incrementally. There are two additional items which must be addressed in computation: directionality of the incremental transformation strain and consistency of the total martensite fraction.

First, to calculate the incremental inelastic transformation strain, we must ensure that the sign of the strain is properly chosen. If the local stress state is found to be in the martensitic transformation strip, and the change from the last step is in the direction of transformation, the new value of ξ is computed and the incremental transformation shear strain is in the direction of the corresponding shear stress. On the other hand, if the local stress state is in the austenitic strip and meets the conditions for reverse transformation, the incremental transformation strain is always in the direction that reduces the existing transformation strain, regardless of the actual direction of stress. Taking this detail into account is crucial in case of complicated loading histories. To illustrate this point, let us consider, for example, the two thermomechanical loading paths in Fig. 8, Γ_1 (ABCDEF) and Γ_2 (ABGHIL). σ is either σ_L or σ_M on a given microplane.

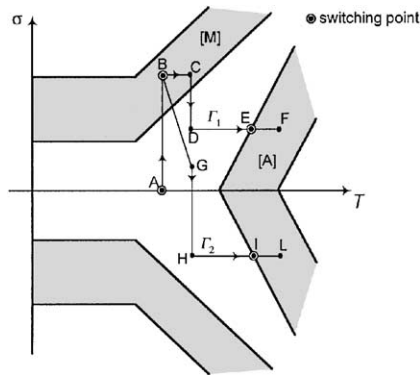


Fig. 8. Example of how the loading path can affect the direction of the increment of inelastic strain.

If we assume that for both Γ_1 and Γ_2 the initial value of ζ is 0, points E and I (where the two paths enter the [A] region) are characterized by the same value of ζ , which is the value reached at point B, common to the two paths (B is the last switching point before E and I). In the two segments EF and IL, ζ decreases by the same amount, but in EF the incremental inelastic strain produced is in the direction opposite to the direction of σ , while in IL the incremental inelastic strain and σ have the same direction.

In addition, since ζ is computed independently on planes of different orientations, consistency of this model necessitates a constraint on the total value of ζ . Such a constraint is expressed in the following form:

$$\zeta_i \geq 0, \quad \sum_i^N \zeta_i \leq 1, \tag{4.10}$$

where ζ_i is the martensite fraction computed on the i th microplane, and N is the number of microplanes used for the numerical integration of Eq. (3.5). Constraint (4.10) is employed at each incremental step. When the total martensite fraction reaches unity, transformation stops and elastic constitutive laws are used until the condition for reverse transformation is achieved.

Examples with the microplane model for SMA response will be shown in the next section.

4.4. Effect of normal components of stress

Experimental tests on SMA have shown very early (Kulin et al., 1952; Burkart and Read, 1953) a significant asymmetry of the material response in tension and compression. As confirmed later by numerous other studies, the compressive stress required for stress-induced martensitic transformation is considerably higher than the tensile stress at transformation for most alloy systems (e.g. Gall et al., 1998) (although the opposite situation has been observed for several different alloys (Sakamoto et al., 1979)). Included in the sample calculations of Section 5 is one additional refinement of the

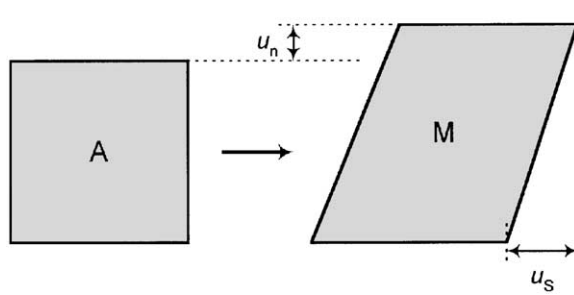


Fig. 9. Schematic representation of transformation from austenite to martensite.

microplane model for SMA, introduced in order to capture the asymmetry of response in tension and compression. We will not address in detail the crystallographic source of such a behavior. However, the underlying mechanism that causes this effect can be intuitively understood in the following way. As shown schematically in Fig. 9, the shear deformation corresponding to martensitic transformation can be accompanied by a small displacement component (u_n) in the direction normal to the plane of shear. A normal component of stress in the direction of displacement u_n will favor the martensitic transformation, while a normal component of stress in the opposite direction will oppose it.

The microplane SMA algorithm can be modified to account for the effect of this normal strain. The simplest first approximation is to introduce a dependence of the microplane kinetic law on the normal component of stress acting on each microplane. At this stage, only a simple method to accomplish this effect is proposed, in order to illustrate qualitatively reasonable results. We assume that the normal component of stress will shift the transformation strips $[A]$ and $[M]$ on the phase diagram, similar to an approach taken by Tanaka et al. (1995a,b). This effect can be obtained by introducing the following relationships:

$$\begin{aligned}
 \sigma_{cr}^s &= \sigma_{cr0}^s + \alpha \sigma_N, \\
 \sigma_{cr}^f &= \sigma_{cr0}^f + \alpha \sigma_N, \\
 A_s &= A_{s0} + \beta \sigma_N, \\
 A_f &= A_{f0} + \beta \sigma_N,
 \end{aligned}
 \tag{4.11}$$

where σ_{cr0}^s , σ_{cr0}^f , A_{s0} , A_{f0} , α and β are determined empirically. Note that the signs of α and β determine whether the presence of normal stress will favor or oppose the transformation and therefore depend on the sign of u_n . (Note that here u_n is introduced with the only purpose of giving a physical justification of parameters α and β , which are, however, determined empirically and not through a precise model of their dependence on u_n).

Introducing this simple dependence of the kinetic law on the normal stress renders the model capable of reproducing the asymmetric material response in tension and in

compression observed in experiments. The numerical example in Section 5.3 illustrates this feature. In the uniaxial case, when the material is loaded in tension and in compression, the normal components of stress on the microplanes change sign. Therefore, the martensitic transformation will be easier in tension for a material characterized by a positive u_n , while it will be easier in compression for a material characterized by a negative u_n .

We conclude the presentation of the SMA microplane model with an observation on the hydrostatic effect. It is recognized that although the thermoelastic transformation of an SMA is nearly volume conserving, a small volumetric strain is observed in nearly all cases. This volumetric strain causes the material response to depend on the hydrostatic stress level (Gall et al., 1998) which must be considered in a three-dimensional model. The dependence of the kinetic law on the normal stress given by Eq. (4.11) introduces automatically a dependence of the overall material response on the hydrostatic pressure. Applying hydrostatic pressure corresponds in fact to applying a uniform normal stress on every microplane and therefore it has an effect in the present model. This is a clear example of one of the advantages of using the microplane model: triaxial phenomena can be naturally reproduced, due to the interaction of the microplanes. The numerical examples in Section 5.4 show how the presence of a pre-applied hydrostatic pressure affects the value of deviatoric stress required to trigger the martensitic transformation. At this stage, we do not directly address the hydrostatic effect in quantitative terms. Rather, we limit ourselves to showing in a qualitative way that the microplane approach offers a solid basis for also tackling this aspect of SMA. For an accurate quantitative model of the effect of triaxial stress states on the crystallographic transformation, it will probably be necessary to introduce a refined form of relations (4.11) such as

$$\begin{aligned}
 \sigma_{\text{cr}}^{\text{s}} &= \sigma_{\text{cr}0}^{\text{s}} + \alpha\sigma_{\text{D}} + \gamma_1\sigma_{\text{V}}, \\
 \sigma_{\text{cr}}^{\text{f}} &= \sigma_{\text{cr}0}^{\text{f}} + \alpha\sigma_{\text{D}} + \gamma_1\sigma_{\text{V}}, \\
 A_{\text{s}} &= A_{\text{s}0} + \beta\sigma_{\text{D}} + \gamma_2\sigma_{\text{V}}, \\
 A_{\text{f}} &= A_{\text{f}0} + \beta\sigma_{\text{D}} + \gamma_2\sigma_{\text{V}},
 \end{aligned} \tag{4.12}$$

where the effect of the volumetric stress is decoupled from the effect of the deviatoric parts of the normal stress components on the microplanes, in order to give the model enough flexibility to take into account both the normal strain associated with the martensitic transformation on a given plane and the overall volume change. Full development and implementation of relationships such as Eq. (4.12) are left to future work.

5. Numerical examples

This section presents some basic and a few advanced numerical tests of the developed SMA microplane model. In these tests, we will consider a polycrystalline shape memory alloy characterized by the following material properties, derived from the data given

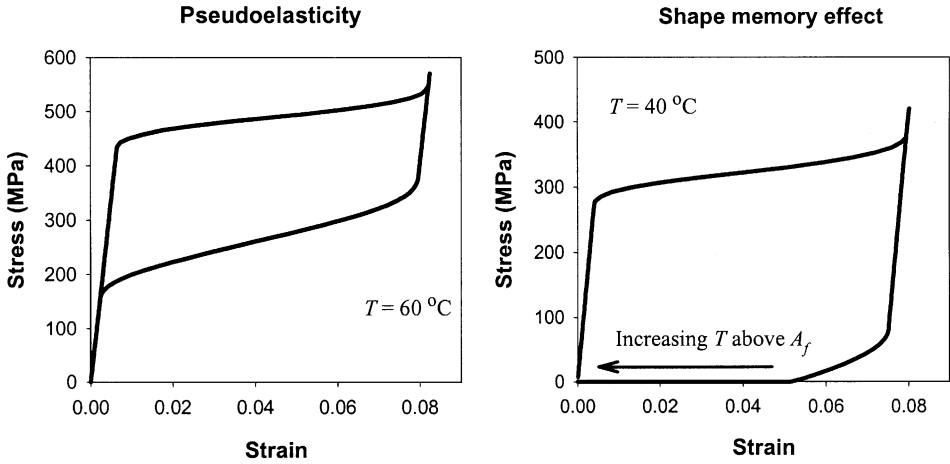


Fig. 10. Pseudoelasticity and shape memory effect for Nitinol by the microplane model.

by Dye (1990) and Liang (1990) for a Nitinol alloy (Ni₅₅Ti):

$$\begin{aligned}
 E &= 52 \times 10^3 \text{ MPa (shear modulus),} \\
 M_f &= 9^\circ\text{C}, \quad M_s = 18.4^\circ\text{C}, \quad A_s = 34.5^\circ\text{C}, \quad A_f = 49^\circ\text{C}, \\
 C_M &= \frac{8}{2} \text{ MPa}/^\circ\text{C}, \quad C_A = \frac{13.8}{2} \text{ MPa}/^\circ\text{C}, \\
 \sigma_s^{cr} &= \frac{100}{2} \text{ MPa}, \quad \sigma_f^{cr} = \frac{170}{2} \text{ MPa}, \\
 \varepsilon_L &= 0.06.
 \end{aligned}
 \tag{5.1}$$

The foregoing values are obtained by adapting to our model the phase diagram defined in terms of uniaxial quantities and used by Brinson (1993) for numerical computation with a one-dimensional model. The SMA microplane model requires a phase diagram in terms of shear quantities on the microplane as discussed in Section 4.2. Such a phase diagram can be obtained from that employed for a tensile model by considering that in the uniaxial case the maximum resolved shear is half of the absolute value of the uniaxial stress. Therefore, the factor 1/2 must be introduced to modify the parameters for the phase diagram, yielding the values in Eq. (5.1). The variation of elastic modulus with martensite fraction is neglected here for the sake of simplicity.

5.1. Uniaxial thermomechanical loading histories

Fig. 10 shows tests of pseudoelasticity and shape memory effect for Nitinol alloy (Ni₅₅Ti). The two curves are in good qualitative and quantitative agreement with the results of Dye (1990) and Liang (1990) and similar results for other shape memory alloys. Fig. 11 shows the agreement between the model and some experimental results presented by Liang (1990) for $T = 50^\circ\text{C}$ and -10°C . All the previously developed

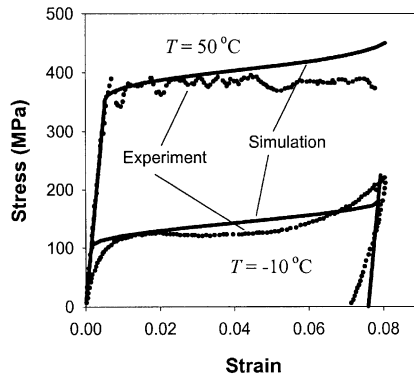


Fig. 11. Experimental and numerical results for the same material considered in Fig. 10, at $T=50^\circ$ and -10° .

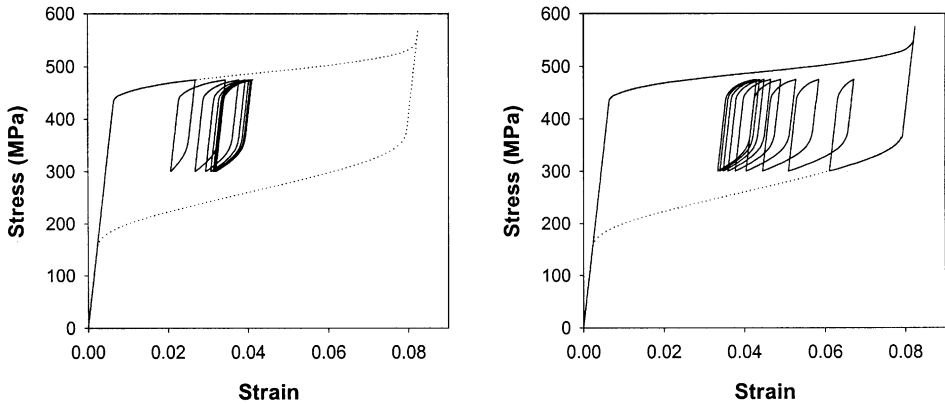


Fig. 12. More complex uniaxial loading histories. Loop attractors for cycling loading.

three-dimensional SMA models can of course reproduce 1-D behavior adequately. The real test of a model comes in more difficult loading situations which follow.

5.2. Cyclic loading histories

Figs. 12 and 13 show the prediction of material response for more complex uniaxial loading histories. Fig. 12 refers to the case in which the material, after loading, is partially unloaded and then subjected to cyclic loading. The model can capture the existence of closed-loop attractors for sustained cyclic loading (Ivshin and Pence, 1994a; Bekker and Brinson, 1998). The same closed loop is approached, from two opposite sides, in the two cases shown in Fig. 12(a) and (b). For comparison, the basic loading–unloading behavior with complete martensitic transformation is also reproduced in the figure. In Fig. 13, the material is subjected to partial unloading and then stress cycling

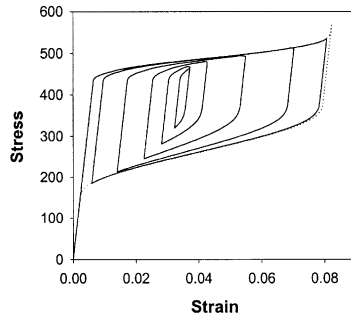


Fig. 13. Stress cycling with gradually diminishing range of stress.

with gradually diminishing range of stress, accurately reproducing material response (Plotnikov et al., 1988).

5.3. Material response in tension and compression

A very important response seen experimentally for SMAs is the tension–compression asymmetry. Such asymmetry, which is caused by different variants being activated under tension and compression, can become exaggerated in the case of textured polycrystalline materials. Here we do not attempt to capture the microscale phenomena, but illustrate that the kinetics in the SMA microplane model can easily be modified to accommodate asymmetry. We implement the simple technique explained in Section 4.4. In our example, the material is loaded in tension up to a value of stress at which all the austenite is transformed into martensite. Then the loading is reversed and the material is loaded in compression. Fig. 14 shows the material response for such a loading history as measured experimentally by Lim and McDowell (1999) in a test on Ni–Ti alloy with the near equiatomic composition (49.20 at% Ti–50.80 at% Ni). The same figure also shows the response obtained with the microplane model. In this example, the microplane model accounts for the effect of the normal component of stress on the microplanes (with $\alpha = 0.16$, $\beta = 0.02$). The material parameters have been adjusted slightly from those listed in Eq. (5.1) to fit the experimental data for this different alloy.

5.4. Effect of hydrostatic pressure

As discussed in Section 4.4, when the kinetic law is made to depend on the normal component of stress on each plane, the overall material response is automatically made dependent on the applied hydrostatic pressure. Fig. 15 illustrates this effect by comparing stress–strain curves for three cases in which the material is subjected to different values of hydrostatic pressure. A hydrostatic pressure σ_V^h is applied and then the material is loaded and unloaded with an additional tensile stress, while keeping σ_V^h constant. To easily compare the three curves obtained for different values of σ_V^h

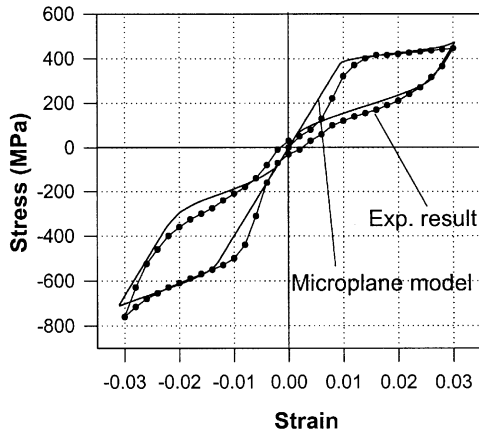


Fig. 14. Stress–strain response during uniaxial cycling (Lim and McDowell, 1999) and numerical result with the microplane model.

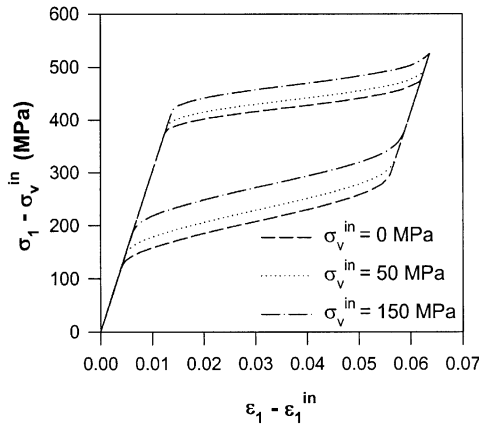


Fig. 15. Effect of hydrostatic pressure.

we plot $\sigma_1 - \sigma_v^h$ versus $\epsilon_1 - \epsilon_1^h$, where ϵ_1^h is the strain in the x_1 direction due to σ_v^h . Fig. 14 clearly shows that the deviatoric stress required to trigger stress-induced martensitic transformation in tension is higher when the hydrostatic pressure is applied to the material beforehand. Such a result is generally consistent for SMA materials shown to have a positive volume change upon transformation. Without the normal stress dependence in the kinetic law (from Eq. (4.11)) a hydrostatic pressure applied in advance has no effect and the three curves would be identical. As previously mentioned, this example shows only qualitatively one possible way to handle the effect of hydrostatic pressure in the microplane model. For materials with texturing or other effects causing inconsistent trends with hydrostatic pressure (Gall et al., 1998; Jacobus et al., 1996) a

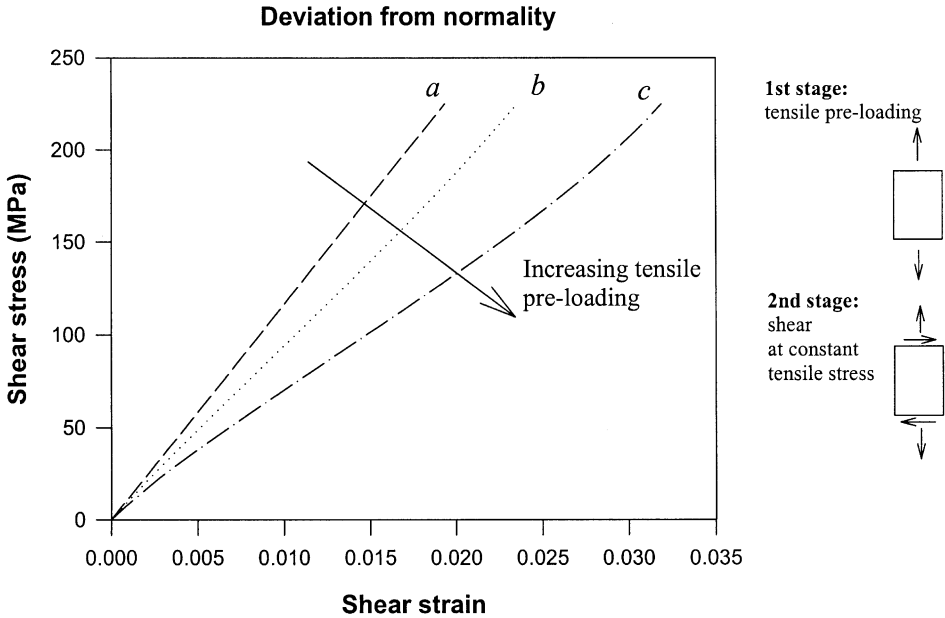


Fig. 16. Overall shear stress vs. overall shear strain, for a material previously subjected to tensile pre-loading.

different approach would be required. An accurate quantitative tuning of this effect is beyond the scope of this paper.

5.5. 3-D cases: nonproportional loading histories

Fig. 16 shows the results calculated for an SMA subjected to tensile pre-loading and then to shear at constant tensile stress. These results are obtained with the basic microplane model developed, without the additional modifications to the kinetic law made in Section 4.4 (and Sections 5.3 and 5.4). A nonproportional two-dimensional loading history as in Fig. 16 is considered to show an apparent deviation from normality for the SMA microplane model. After the tensile load is applied, an associated flow rule based on a macroscale J_2 potential would predict an elastic tangential shear stiffness regardless of the amount of tensile pre-stress. In the results obtained with the microplane model, the tangential shear stiffness is reduced if the shear stress is applied after the material is loaded in tension into the inelastic region.

The three curves in Fig. 16 correspond to the response in shear for three different levels of pre-stress. Curve *a* is obtained for the case in which the pre-loading is such that the martensitic transformation does not yet occur and the tangential shear modulus is therefore the elastic shear modulus. For curves *b* and *c*, the amount of pre-applied stress is enough to induce martensitic transformation. When the direction of incremental applied stress is changed to shear, the resolved incremental component of shear stress on some microplanes will have the same direction as in the first stage of loading, in which

the tensile stress is applied. Therefore, the material will continue transforming on such microplanes and the overall macroscopic response will be inelastic and characterized by a reduced tangential shear stiffness. Pre-applying compression would produce an analogous behavior.

The model thus appears to be qualitatively suitable to describe the deviation from normality observed in Lim and McDowell's (1999) experiments, called the vertex effect. The ability of the 3-D SMA model to capture this experimentally observed behavior is an important novel feature.

6. Conclusions

The existing constitutive models for SMA are usually developed following either a phenomenological or a micromechanical approach. The SMA microplane model proposed in this paper represents an ideal compromise. By considering the possibility of martensitic transformation on several planes of different orientation, and by obtaining the overall transformation strain as a superposition of shear-induced transformation strains, the new model can reproduce the actual physical behavior of SMA materials in a closer way than other phenomenological models. Nevertheless, the model can be implemented by simply considering 1-D phenomenological constitutive laws on each plane, thus remaining conceptually simpler than a micromechanics-based model. Note again that the model presented here is a macroscale, polycrystalline SMA model: the microplanes provide a mechanism to build a more consistent 3-D SMA model from a robust 1-D SMA model, but do not represent actual crystallographic transformation planes.

As seen in Section 4, the microplane model provides a very efficient computational framework for extending a 1-D phenomenological model to the 3-D case. The numerical examples considered show the predicted material response to be in good qualitative agreement with the behavior observed experimentally. Importantly, we have considered not merely simple uniaxial loading with complete transformation, but also complex loading histories. A robust kinetic law is used, to allow easy modification as needed. It is illustrated that asymmetric tension–compression and hydrostatic loading effects can be accommodated by including a dependence of the microplane kinetic law on the normal component of stress on the microplanes (or on the volumetric stress). Some SMA models based on the thermodynamics framework would require substantial changes to capture these features.

A very important feature of SMA transformation under multiaxial loading is that J_2 or Drucker–Prager models with associated flow rules are not obeyed in the case of nonproportional loading. It is shown here that the model developed within the microplane framework exhibits apparent deviations from the normality rule (with vertex effect) in the case of nonproportional loading and therefore captures the mechanical behavior of SMAs realistically.

Finally, it should be noted that the SMA microplane model provides a useful platform for further advances. First, the macroscale polycrystalline model proposed here can be further refined on the basis of experimental data and can be utilized in large-scale

numerical computations (e.g., finite element analyses). Second, the microplane model offers an excellent opportunity to address the single crystal behavior on the microscale. The microplanes can be chosen to coincide with the martensitic plate habit planes and the shear directions can be chosen to be aligned with the known transformation directions on those habit planes. Although this microscale approach may require significant reformulation of the microplane theory, the success of the present macroscale model suggests the microplane approach as quite an appealing device for capturing complex multidimensional single crystal behavior more realistically than before.

Acknowledgements

The work of the authors was partially supported under NSF grants cms-9501792 (LCB) and cms-9732791 (MB and ZPB) to Northwestern University.

References

- Auricchio, F., Sacco, E., 1999. A temperature-dependent beam for shape-memory alloys: constitutive modelling, finite-element implementation and numerical simulations. *Comput. Method Appl. Math.* 174 (1–2), 171–190.
- Auricchio, F., 1995. Shape-memory alloys: applications, micromechanics, macromodeling and numerical simulations. Ph.D. Thesis, University of California at Berkeley, Berkeley, CA.
- Batdorf, S.B., Budiansky, B., 1949. A Mathematical Theory of Slip Based on the Concept of Slip. NACA TN1871.
- Bažant, Z.P., 1984. Microplane model for strain controlled inelastic behavior. Chapter 3. In: Desai, C.S., Gallagher, R.H. (Eds.), *Mechanics of Engineering Materials*. Wiley, London, pp. 45–59.
- Bažant, Z.P., Oh, B.H., 1985. Microplane model for progressive fracture of concrete and rock. *J. Eng. Mech.-ASCE* 111 (4), 559–582.
- Bažant, Z.P., Oh, B.H., 1986. Efficient numerical integration on the surface of a sphere. *Z. Angew. Math. Mech. (ZAMM, Berlin)* 66 (1), 37–49.
- Bažant, Z.P., Prat, P., 1987. Creep of anisotropic clay: new microplane model. *ASCE J. Eng. Mech.* 103 (7), 1050–1064.
- Bažant, Z.P., Prat, P.C., 1988a. Microplane model for brittle-plastic material. 1. Theory. *J. Eng. Mech.—ASCE*. 114 (10), 1672–1687.
- Bažant, Z.P., Prat, P.C., 1988b. Microplane model for brittle-plastic material. 2. Verification. *J. Eng. Mech.—ASCE*. 114 (10), 1689–1702.
- Bažant, Z.P., Xiang, Y.Y., Prat, P.C., 1996. Microplane model for concrete. 1. Stress–strain boundaries and finite strain. *J. Eng. Mech.-ASCE* 122 (3), 245–254.
- Bažant, Z.P., Caner, F.C., Carol, I., Adley, M.D., Akers, S.A., 2000. Microplane model M4 for concrete—I. Formulation with work-conjugate deviatoric strains. *ASCE J. Eng. Mech.* 126 (9), 944–953.
- Bekker, A., Brinson, L.C., 1998. Phase diagram based description of the hysteresis behavior of shape memory alloys. *Acta Mater.* 46 (10), 3649–3665.
- Birman, V., 1997. Review of mechanics of shape memory alloy structures. *Appl. Mech. Rev.* 50, 629–645.
- Borden, T., 1996. Shape memory alloy: forming a tight fit. *Mech. Eng.* 113 (10), 66–72.
- Boyd, J.G., Lagoudas, D.C., 1996a. A thermodynamic constitutive model for the shape memory materials. Part I. The monolithic shape memory alloy. *Int. J. Plast.* 12, 805–841.
- Boyd, J.G., Lagoudas, D.C., 1996b. A thermodynamic constitutive model for the shape memory materials. Part II. The SMA composite material. *Int. J. Plast.*, V. 12 (7), 843–873.

- Boyd, J.G., Lagoudas, D.C., 1994. Thermomechanical response of shape memory composites. *J. Intell. Matl. Syst. Struct.* 5 (3), 333–346.
- Brinson, L.C., 1993. One dimensional constitutive behavior of shape memory alloys: thermomechanical derivation with non-constant material functions. *J. Intell. Matl. Syst. Struct.* 4 (2), 229–242.
- Brinson, L.C., Huang, M.S., 1996. Simplifications and comparisons of shape memory alloy constitutive models. *J. Intell. Matl. Syst. Struct.* 7, 108–114.
- Brocca, M., Bažant, Z.P., 2000. Microplane model and metal plasticity. *Appl. Mech. Rev.* 53 (10), 265–281.
- Budiansky, B., Wu, T.T., 1962. Theoretical prediction of plastic strains in polycrystals. *Proc. 4th US Natl. Congr. Appl. Mech.*, pp. 1175–1185.
- Burkart, M.W., Read, T.A., 1953. *Trans. TMS-AIME* 197, 1516–1524.
- Carol, I., Bažant, Z.P., 1997. Damage and plasticity in microplane theory. *Int. J. Solids Struct.* 34 (29), 3807–3835.
- Dye, T.E., 1990. An experimental investigation of the behavior of nitinol. MS Thesis, Virginia Tech.
- Gall, K., Sehitoglu, H., Maier, H.J., Jacobus, K., 1998. Stress-induced martensitic phase transformations in polycrystalline CuZnAl shape memory alloys under different stress states. *Metall. Mater. Trans. A* 29A, 765–773.
- Gao, X., et al., 2000. A multivariant micromechanical model for SMAs: Part 1: Crystallographic issues for single crystal model. *Int. J. Plasticity* 16, 1345–1369.
- Goo, B.C., Lexcelent, C., 1997. Micromechanics based modeling of two-way memory effect of a single crystalline shape memory alloy. *Acta Metall.* 45, 727–737.
- Govindjee, S., Hall, G.J., 2000. A computational model for shape memory alloys. *Int. J. Solids Struct.* 37 (5), 735–760.
- Graesser, E.J., Cozzarelli, F.A., 1991. Shape-memory alloys as new materials for aseismic isolation. *J. Eng. Mech.* 117 (11), 2590–2608.
- Hill, R., 1965. Continuum micro-mechanics of elastoplastic polycrystals. *J. Mech. Phys. Solids* 13 (2), 89–102.
- Hill, R., 1966. Generalized constitutive relations for incremental deformation of metal crystals by multislip. *J. Mech. Phys. Solids* 14 (4), 95–102.
- Huang, M.S., Brinson, L.C., 1998. A multivariant model for single crystal shape memory alloys. *J. Mech. Phys. Solids* 46, 1379–1409.
- Ivshin, Y., Pence, T.J., 1994a. A thermomechanical model for a one variant shape memory material. *J. Intell. Matl. Syst. Struct.* 5, 455–473.
- Ivshin, Y., Pence, T.J., 1994b. A constitutive model for hysteretic phase transition behavior. *Int. J. Eng. Sci.* 32, 681–704.
- Jacobus, K., Sehitoglu, H., Balzer, M., 1996. Effect of stress state on the stress-induced martensitic transformation in polycrystalline NiTi alloy. *Metall. Mater. Trans.* 27, 3333.
- Kröner, E., 1961. *Acta Metall.* 9, 155.
- Kulin, S.A., Cohen, M., Averbach, B.L., 1952. *J. Met.* 4, 661–670.
- Lagoudas, D.C., Boyd, J.G., Bo, Z., 1994. Micromechanics of active composites with SMA fibers. *ASME J. Eng. Mater. Technol.* 116, 337–347.
- Lagoudas, D.C., Bo, Z., Qidwai, M.A., 1996. A unified thermodynamic constitutive model for sma and finite element analysis of active metal matrix composites. *Mech. Composite Mater. Struct.* 3, 153–179.
- Liang, C., 1990. The constitutive modeling of shape memory alloys. Ph.D. Thesis, Virginia Tech.
- Liang, C., Rogers, C.A., 1990. One-dimensional thermomechanical constitutive relations for shape memory materials. *J. Intell. Matl. Syst. Struct.* 1 (2), 207–234.
- Liang, C., Rogers, C.A., 1992. A multi-dimensional constitutive model for shape memory alloys. *J. Eng. Math.* 26, 429–443.
- Lim, T.J., McDowell, D.L., 1999. Mechanical behavior of an Ni–Ti shape memory alloy under axial–torsional proportional and nonproportional loading. *J. Eng. Mater. Technol.—Trans. ASME* 121 (1), 9–18.
- Lin, T.H., Ito, M., 1965. Theoretical plastic distortion of a polycrystal aggregate under combined and reversed stresses. *J. Mech. Phys. Solids* 13 (2), 103–115.
- Lin, T.H., Ito, M., 1966. Theoretical plastic stress-strain relationship of polycrystal. *Int. J. Eng. Sci.* 4, 543–561.

- Lu, L., Aernoudt, E., Wollants, P., Humbeeck, J.v., Delaey, L., 1990. Simulation of transformation hysteresis. *Z. Metall.* 81 (H9), 613–622.
- Lu, Z.K., Weng, G.J., 1997. Martensitic transformations and stress–strain relations of shape-memory alloys. *J. Mech. Phys. Solids* 45, 1905–1928.
- Lubliner, J., Auricchio, F., 1996. Generalized plasticity and shape memory alloys. *Int. J. Solids Struct.* 33 (7), 991–1003.
- Oberaigner, E.R., Tanaka, K., Fisher, F.D., 1996. Investigation of the damping behavior of vibrating shape memory alloy rod using a micromechanical model. *Smart Mater. Struct.* 3, 456–563.
- Otsuka, K., Wayman, C.M., 1998. *Shape Memory Materials*. Cambridge University Press, Cambridge, 284pp.
- Pande, G., Sharma, K., 1983. Multilaminate model of clays—A numerical evaluation of the influence of rotation of principal axes. *ASCE J. Eng. Mech.* 109 (7), 397–418.
- Pande, G.N., Xiong, W., 1982. An improved multi-laminate model of jointed rock masses. In: Dungar, R., Pande, G.N., Studer, G.A. (Eds.), *Proc., Intl. Symp. Numerical Model Geomechs.*, Zurich, September 1982, pp. 218–226.
- Patoor, E., Eberhardt, A., Berveiller, M., 1988. Thermomechanical behaviour of shape memory alloys. *Arch. Mech.* 40 (5–6), 775–794.
- Patoor, E., Eberhardt, A., Berveiller, M., 1993. Micromechanical modelling of superelasticity in shape memory alloys. *Pitman Res. Notes Math. Ser.* 296, 38–54.
- Patoor, E., Eberhardt, A., Berveiller, M., 1994. Micromechanical modelling of the shape memory behavior. In: Brinson, L.C., Moran, B. (Eds.), *Mechanics of Phase Transformation and Shape Memory Alloys*, ASME AMD Vol. 189, pp. 23–37.
- Plotnikov, V.A., Monasevich, L.A., Paskal, Yu.I., 1988. Acoustic emission caused by precipitation hardening during the thermoelastic martensitic transformation. *Phys. Met. Metallogr.* 65 (6), 168–170.
- Prat, P., Bažant, Z.P., 1989. Microplane model for triaxial deformation of soils. In: Pietruszczak, S., Pande, G. (Eds.), *Numerical Models in Geomechanics (NUMOG III)*. Elsevier, Niagara Falls, Canada, pp. 139–146.
- Prat, P., Bažant, Z.P., 1991a. Microplane model for triaxial deformation of saturated cohesive soils. *ASCE J. Geotech. Eng.* 117 (6), 891–912.
- Prat, P., Bažant, Z.P., 1991b. A time dependent microplane model for creep of cohesive soils. In: Adeli, H., Sierakowski, R.L. (Eds.), *Mechanics computing in the 90s and beyond*, Proceedings of the ASCE-EMD Speciality Conference, ASCE, Columbus, OH, USA, pp. 1224–1228.
- Rice, J.R., 1971. Inelastic constitutive relations for solids—an internal-variable theory and its application to metal plasticity. *J. Mech. Phys. Solids* 19 (6), 433–455.
- Sakamoto, H., Tanigawa, M., Otsuka, K., Shimizu, K., 1979. Proceedings of the International Conference on Martensitic Transformations, ICOMAT-79, Cambridge, MA, pp. 633–638.
- Stroud, A.H., 1971. *Approximate Calculation of Multiple Integrals*. Prentice-Hall, Englewood Cliffs, NJ.
- Sun, Q.P., Hwang, K.C., 1993. Micromechanics modelling for the constitutive behavior of polycrystalline shape memory alloys—1, 2. *J. Mech. Phys. Solids* 41 (1), 1–17.
- Tanaka, K., Nagaki, S., 1982. A thermomechanical description of materials with internal variables in the process of phase transitions. *Ing. Arch.* 51, 287–299.
- Tanaka, K., Nishimura, F., Hayashi, T., Tobushi, H., LExcellent, C., 1995a. Phenomenological analysis on subloops and cyclic behavior in shape memory alloys under mechanical and/or thermal loads. *Mech. Mater.* 19, 281–292.
- Tanaka, K., Nishimura, F., Tobushi, H., 1995b. Transformation start lines in TiNi and Fe-based shape memory alloys after incomplete transformations induced by mechanical and/or thermal loads. *Mech. Mater.* 19, 271–280.
- Tanaka, K., Nishimura, F., Matsui, M., Tobushi, H., Lin, P.-H., 1996. Phenomenological analysis of plateaus on stress–strain hysteresis in TiNi shape memory alloy wires. *Mech. Mater.* 24, 19–30.
- Taylor, G.I., 1938. Plastic strain in metals. *J. Inst. Metals* 63, 307–324.
- Vivet, A., LExcellent, C., 1998. Micromechanical modelling for tension–compression pseudoelastic behavior of AuCd single crystals. *EPJ Appl. Phys.* 4 (2), 125–132.
- Wu, X.C., Pence, T.J., 1998. Two variant modeling of shape memory materials: unfolding a phase diagram triple point. *J. Intell. Mater. System Struct.* 9 (5), 335–354.
- Zienkiewicz, O., Pande, G., 1977. Time-dependent multi-laminate model of rocks—a numerical study of deformation and failure of rock masses. *Int. J. Anal. Numer. Methods Geomech.* 1, 219–247.